XX. Physics

SPACE SCIENCES DIVISION

N67-29161

A. A Spectrometer for Simultaneous Observation of the Spectra of Two Nuclei of Different Magnetogyric Ratios, *D. D. Elleman, S. L. Manatt, and C. D. Pearce*

To perform field-sweep heteronuclear double-resonance experiments, one must consider the difference in relative sweep distances (as measured in field units) introduced by the difference of gyromagnetic ratios of the sets of nuclei being studied. Simultaneous observation of the two nuclei would greatly facilitate this type of experiment (SPS 37-41, Vol. IV, pp. 180, 181). We describe herein some modifications to our standard nuclear magnetic resonance (NMR) probes that make this technique feasible.

Ideally, a heteronuclear double-resonance experiment requires a multiple-frequency synthesizer spectrometer with nuclear field stabilization. Therefore, a single spectral line can be continuously observed while one or more types of nuclei in the sample molecule are irradiated by changing the other relevant frequencies. Experiments of this type, previously referred to as INDOR (Ref. 1) experiments, can give significant information on the nuclear-spin energy level schemes and on relaxation phenomenon. It is possible to realize some of the advantages of the ideal spectrometer mentioned above in simple field-sweep double-resonance experiments without the extra complication of nuclear field stabilization. The requisite components and modifications to perform such experiments are: (1) two Varian 4311 RF units of the appropriate frequencies, (2) frequency synchronization between the two RF units, (3) double tuning of the Varian 4331A probe transmitter circuit, (4) double tuning of the Varian 4331A probe receiver circuit, and (5) a convenient means for simultaneously displaying the two nuclear signals when the field is swept.

The basis of our system is a Varian HR-60. In one disposition, the Varian 4311 units were at frequencies of 24.3, 56.4, and 60.0 Mc for a number of ^{31}P-, ^{19}F-, and ^{1}H-containing molecules which we have been studying. The master oscillator crystals were removed from these units and replaced by two Hewlett–Packard 5100A frequency synthesizers. The synthesizers were driven from the same Hewlett–Packard 5100A driver unit. The receiver circuit of a 60-Mc Varian 4331A probe was modified as shown in Fig. 1(a) so as to give a good signal-to-noise

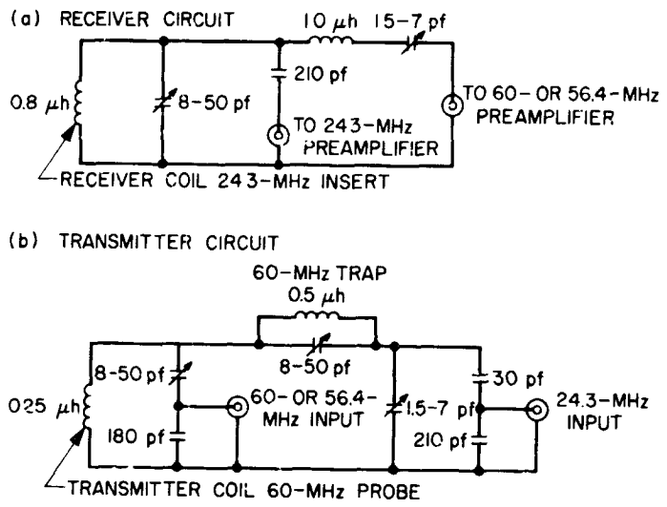

Fig. 1. Receiver and transmitter circuits of Varian 4331A probe modified for dual-frequency operation

value for 24.3 Mc and a somewhat smaller signal-to-noise value at 56.4 Mc and 60.0 Mc. We estimate that the signal-to-noise value at 24.3 Mc was down a factor of only 2 to 3 from that of a standard 24.3-Mc probe. A 24.3-Mc receiver insert was used in the 60-Mc probe so some of the signal-to-noise loss at the proton and fluorine frequencies was gained back from the lower frequency insert, which has about four to five times more turns of wire than 60-Mc inserts. The transmitter circuit of the 60-Mc probe was modified as shown in Fig. 1(b) so as to resonate at 24.3 and either 56.4 or 60 Mc. The additional probe components were housed in two aluminum boxes attached to the probe (Fig. 2). To obtain more RF power in certain decoupling experiments, the output of either Varian 4311 unit was coupled to a Boonton 230A power amplifier, whose output was fed to the probe transmitter circuit. Usually, in simple field-sweep experiments, it was possible to record spectra directly from the output of the Varian 4311 RF phase detectors; however, for certain experiments it was necessary to lock the field through a synchronous detector locked on the tetramethylsilane proton line.

Some simultaneously recorded ^{31}P and ^{1}H spectra of trimethylphosphite, $(CH_3O)_3P$, are shown in Fig. 3(a,b,c). Positive and negative signal enhancements of greater than 10 are evident in Fig. 3(b) and 3(c), respectively. In Fig. 3(d), the ^{31}P frequency-sweep spectrum of this compound was recorded while the field was locked on a tetramethylsilane line and one of the proton lines was irradiated with an audio modulation appropriate to give the most pronounced intensity perturbations of the least intense lines. These are barely visible in Fig. 3(a). The ^{31}P center-band frequency was swept by feeding a negative ramp from a

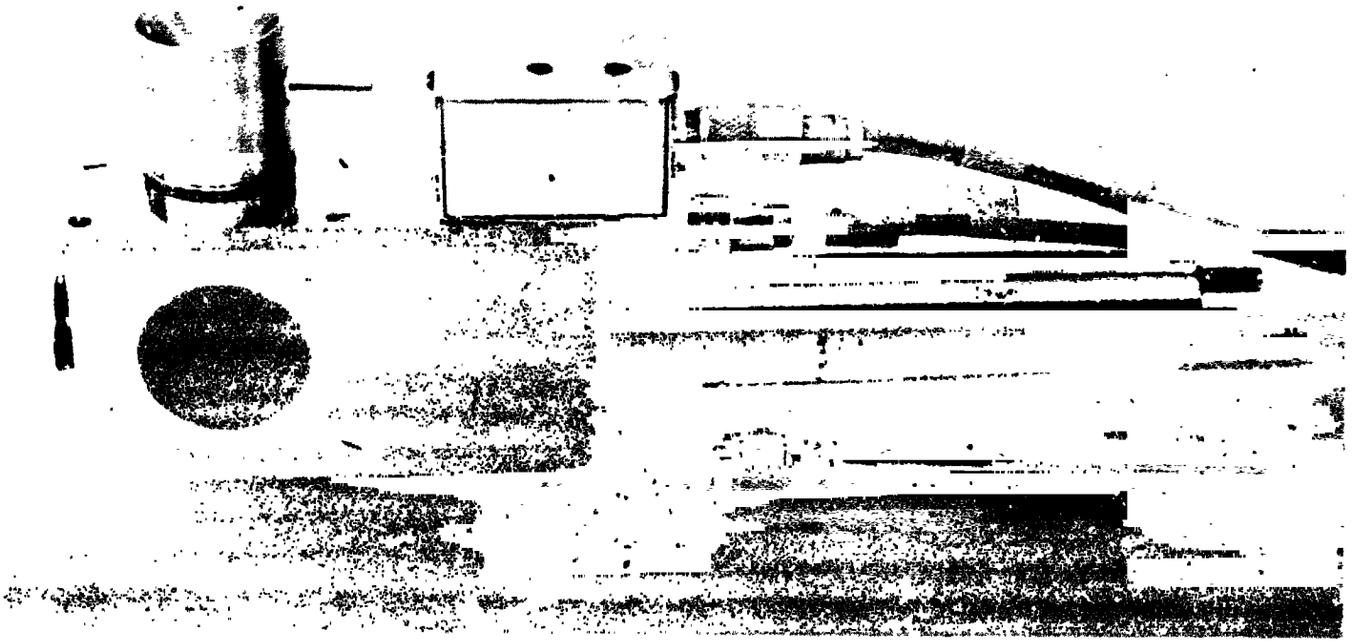

Fig. 2. Modified Varian 4331A probe

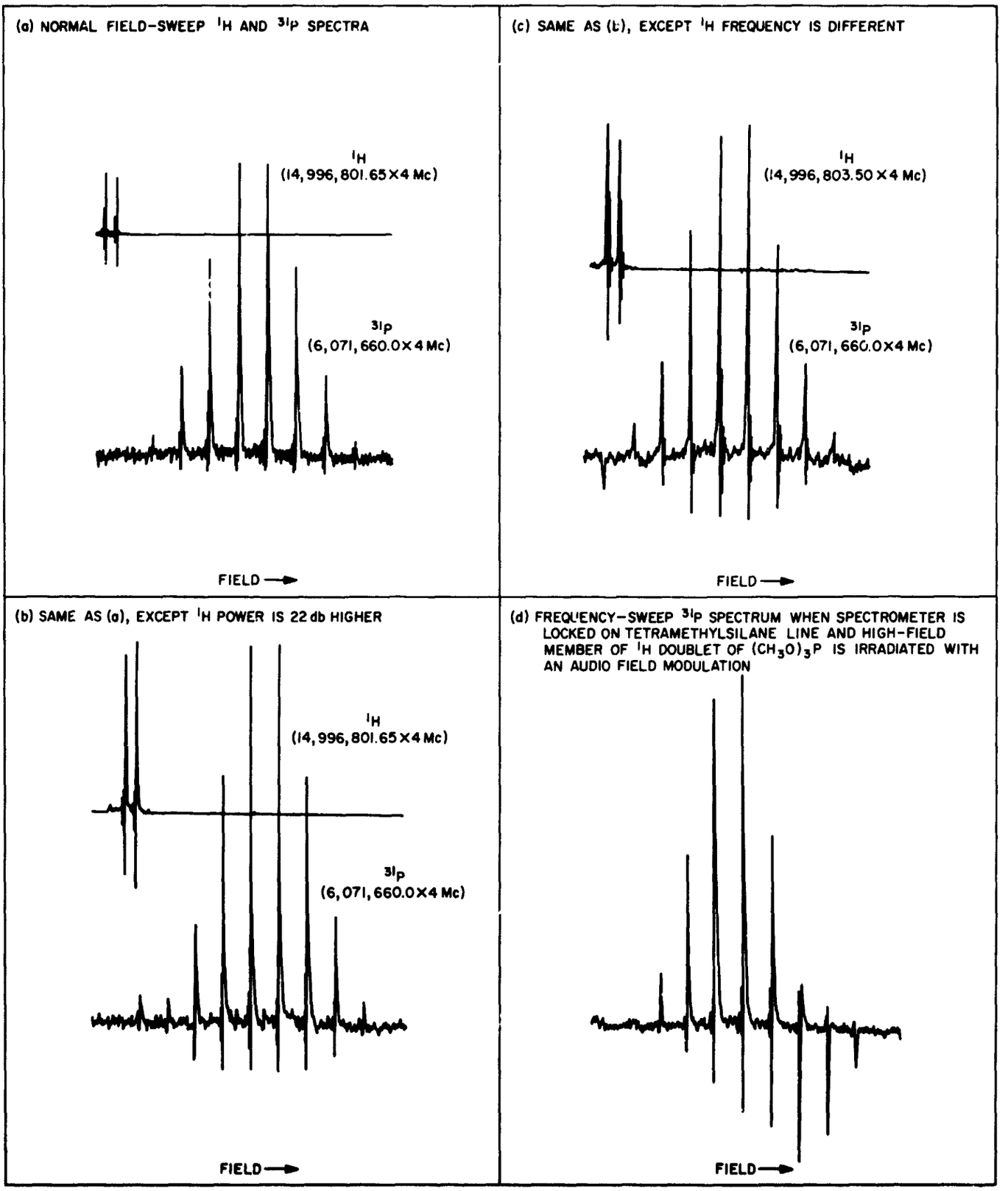

Fig. 3. NMR spectra of $(CH_3O)_3P$ (neat)

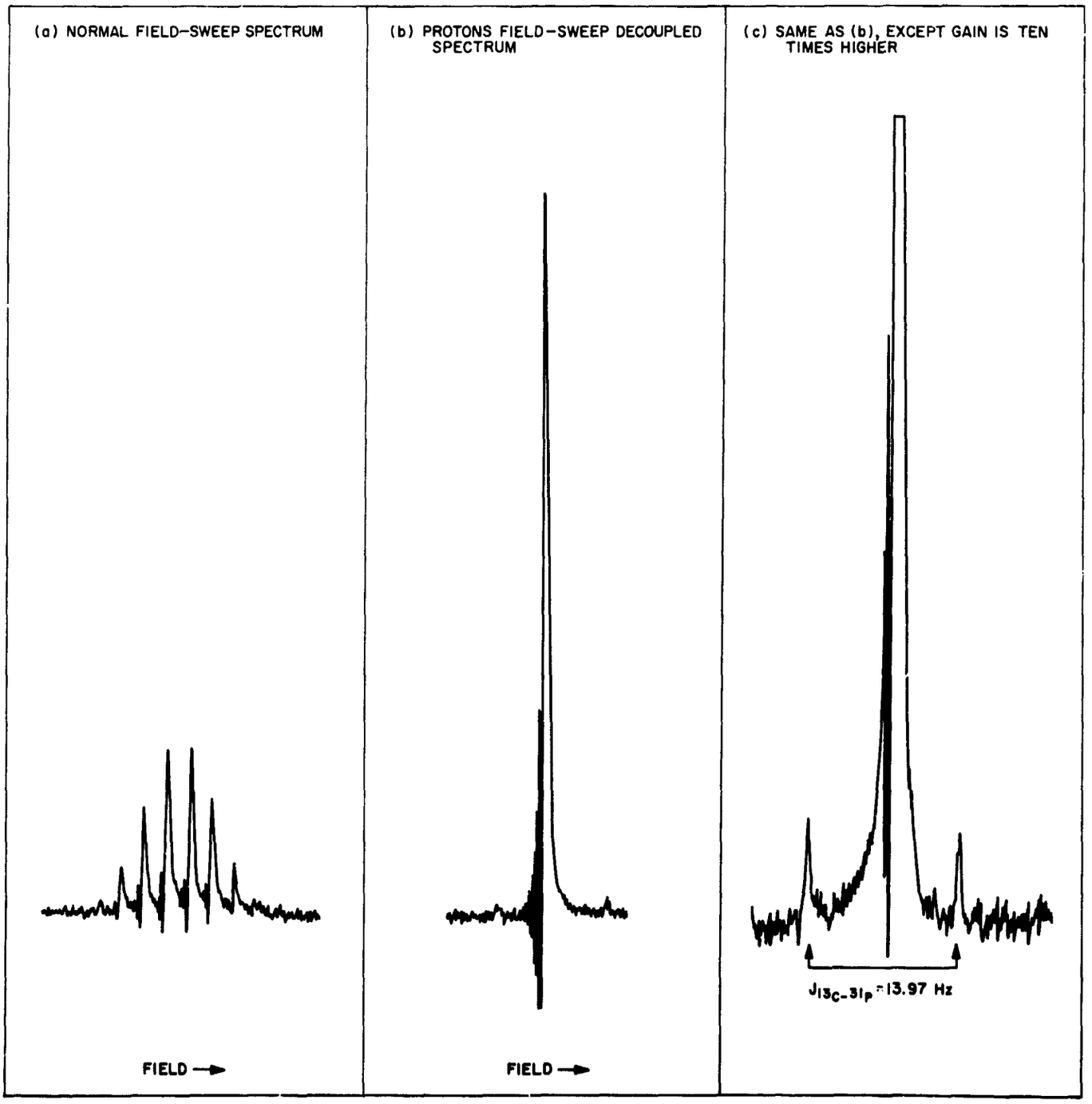

Fig. 4. ^{31}P spectra of $(CH_3)_3P$ (neat)

motor-driven 10-turn pot to the search oscillator of the appropriate frequency synthesizer. On completely decoupling the protons in trimethylphosphite, the ^{31}P signal intensity increased by a factor of 1.5 from that expected for just collapse of the multiplet structure of Fig. 3(a).

Fig. 4(a) shows the field-sweep ^{31}P spectrum of trimethylphosphine, $(CH_3)_3P$; Fig. 4(b) shows the field-sweep completely decoupled spectrum. Note the two weak signals on either side of the main signal. Fig. 4(c) shows the same region at higher gain. The doublet structure we ascribe to a directly bonded ^{13}C–^{31}P coupling of -13.97 ± 0.04 Hz. This assignment is based on two facts: At progressively lower levels of ^1H irradiation, the doublet signals broaden and finally disappear, even though the protons in the molecules $(^{12}CH_3)_3{}^{31}P$ are still completely decoupled. Furthermore, the doublet is not centered about the decoupled ^{31}P signals from the $(^{12}CH_3)_3{}^{31}P$ species because of a ^{31}P isotopic chemical shift of 0.98 ± 0.04 Hz of the $(^{13}CH_3)(^{12}CH_3)_2P$ species. The negative sign is given this ^{13}C–^{31}P coupling relative to the ^{13}C–H coupling because, if the ^1H frequency is increased some 40 Hz, it is observed in field-sweep spectra that the high-field line becomes slightly sharpened and the low-field line becomes significantly broadened. The reverse effect is observed when the ^1H frequency is decreased.

B. Low-Temperature Chromatographic Separation of Some Permanent Gases, *J. King, Jr.*

1. Introduction

The permanent gases argon (Ar), oxygen (O_2), nitrogen (N_2), and methane (CH_4) have been separated on an alumina (Al_2O_3) column at low temperatures. These gases were chosen to obtain experimental evidence in support of the electrostatic theory of physical adsorption (Ref. 2). The fact that they must also be included in any chromatographic atmospheric analysis gives added impetus to the investigations.

In the electrostatic theory, the dominant attractive energy between the gases and the surface was proposed to be (Ref. 2)

$$\Phi_{att} = -\frac{\alpha}{2} E_z^2 \qquad (1)$$

where α is the polarizability of the adsorbed gas, and E_z is the electric-field intensity normal to the surface. There is a unique relationship between the molecular polarizabilities of the chosen gases which allows them to be used as tests for Eq. (1). The diatomic molecules, O_2 and N_2, have two distinct polarizabilities: $\alpha_{\parallel}$ along the internuclear axis, and $\alpha_{\perp}$ normal to the axis. CH_4 has an isotropic polarizability, and its behavior on the surface should be similar to that of a rare gas (e.g., Ar). When O_2 and N_2 are freely rotating, the effective polarizability is an average of $\alpha_{\parallel}$ and $\alpha_{\perp}$ and is defined as (Ref. 3, p. 949).

$$\alpha_{av} = \frac{1}{3}(\alpha_{\parallel} + 2\alpha_{\perp}) \qquad (2)$$

The polarizabilities of the permanent gases are given below, where the molecular diameter σ is included to show that the molecules are of comparable sizes:

Item	Ar	O_2	N_2	CH_4
$\alpha_{\parallel}$, A^3	1.63	2.35	2.38	2.60
$\alpha_{\perp}$, A^3	1.63	1.21	1.45	2.60
α_{av}, A^3	1.63	1.60	1.76	2.60
σ, A	3.40	3.47	3.70	3.82

If Eq. (1) does represent the major attractive force, then O_2 and N_2, when freely rotating on the surface, should behave like Ar since their effective polarizabilities are similar. Conversely, if their rotational motion is hindered, their behavior should deviate from that of Ar. Since N_2 has a large quadrupole moment (Ref. 3, p. 1028), its rotational motion should be affected in a strong electric field. The electric-field quadrupole interaction will tend to align the molecule's internuclear axis with the field. O_2, whose quadrupole moment is rather small (Ref. 3, p. 1028), should be less affected. Under conditions where the interaction is so strong that N_2 ceases to rotate, its behavior on the surface should approach that of CH_4. To observe these effects, the experiments were performed at low temperatures, where the molecules have less kinetic energy.

2. Experimental

Some innovations were made in the ordinary gas chromatography setup. Since the activity of the Al_2O_3 had to be closely controlled, it was necessary to have ultra-dry carrier gas. Any water, even in trace quantities, greatly reduces the activity. Therefore, to eliminate all traces of water, the carrier gas was passed through a molecular sieve trap at liquid-nitrogen temperature prior to sample injection. Temperature variation and control were obtained by automatically maintaining an isopentane

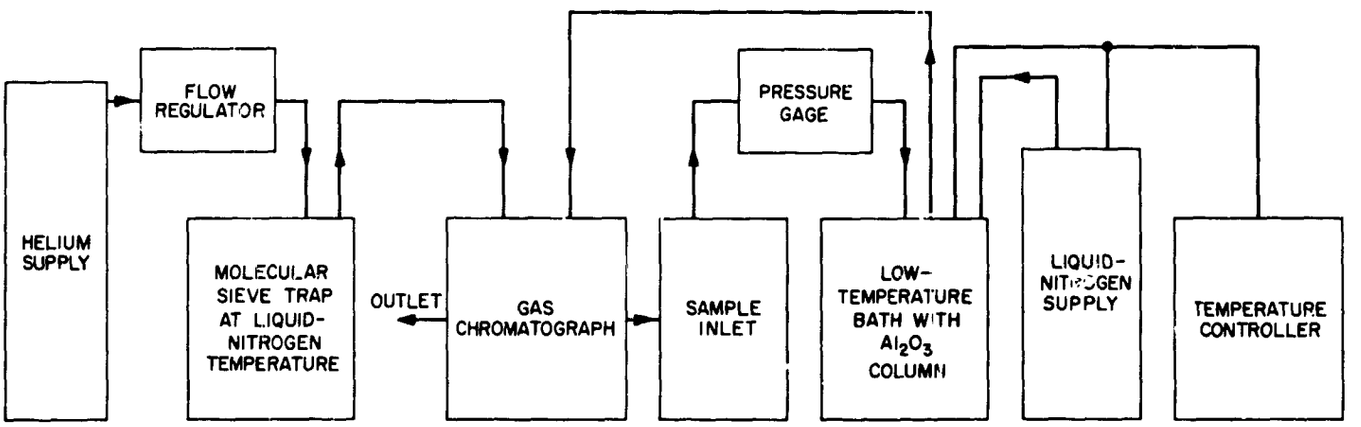

Fig. 5. Block diagram of experimental apparatus

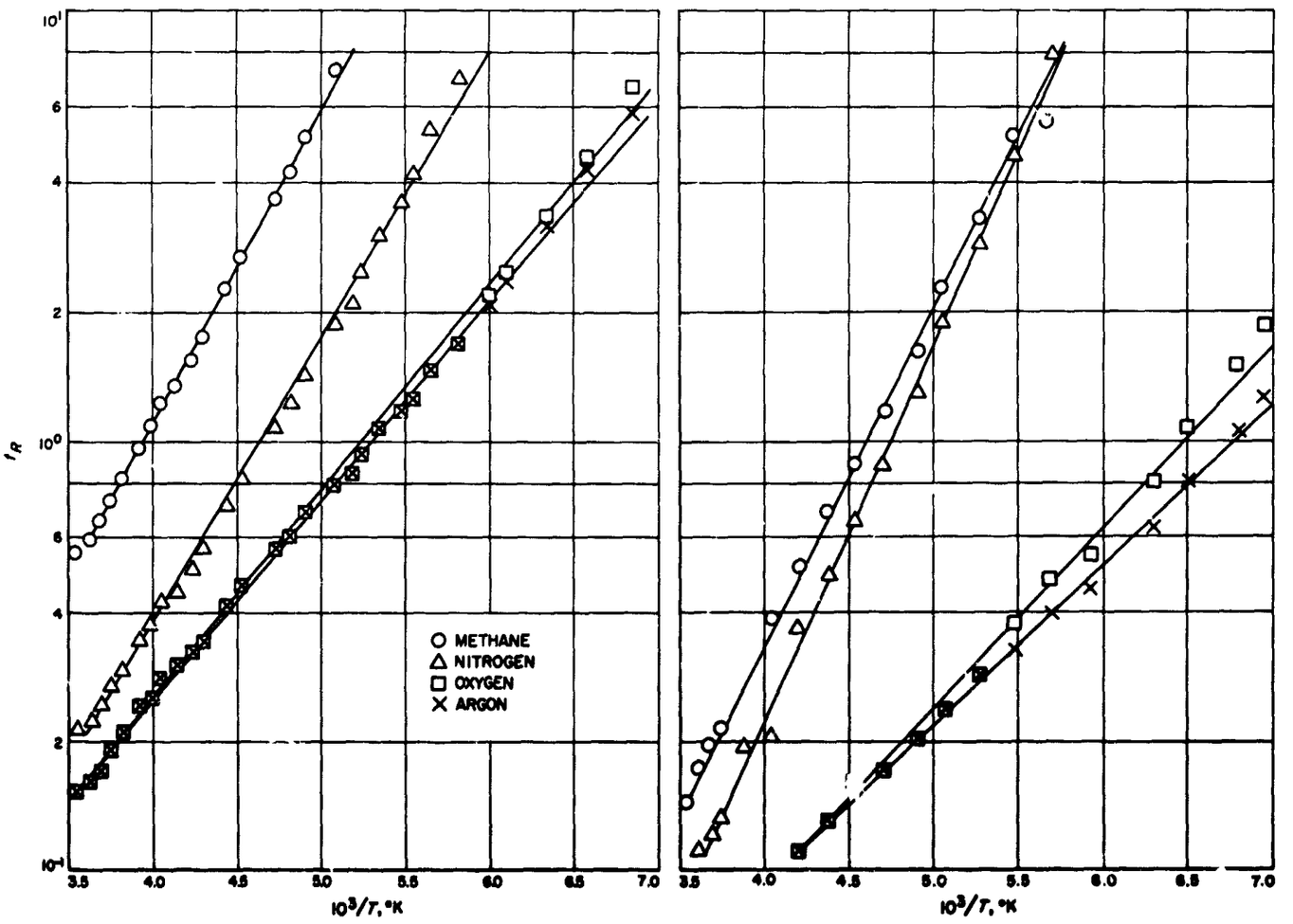

Fig. 6. Chromatographic separations on Al_2O_3 column activated at both 350 and 900°C for 100 hr

bath at the desired temperature. The isopentane was contained in a low-temperature dewar. Inside the dewar was a large copper cylinder with copper tubing wound on its outside. The tubing was connected to a liquid-nitrogen source, which was controlled by a sensing element immersed in the isopentane and an automatic temperature controller. Magnetic stirring was obtained by use of a small propeller attached to the bottom of the copper cylinder and a rotating magnet outside of the dewar. A block diagram of the experimental setup is shown in Fig. 5.

The column was made by coiling 8 ft of quartz tubing to fit into the low-temperature dewar. The column was packed with Alcon Type F-1 activated Al_2O_3 (~150 mesh) by applying compressed air at the inlet and a vacuum at the outlet and vibrating the column by means of a drill motor. The weight of the material in the column was 70.2 g.

The experimental procedure consisted of: (1) activating the column at 350°C for 100 hr in a tubular heater, (2) placing the column in the low-temperature bath, (3) performing the separations over the temperature range (4) replacing the column in the heater and activating at 900°C for 100 hr, and (5) repeating the separations over the temperature range with the newly activated column. All of these functions were performed without discontinuing the flow of the helium carrier gas through the column. The same flow rate was maintained at each temperature by using a flow regulator and systematically readjusting the flow when it deviated by more than 1% from 100 cm^3/min.

3. Results and Discussion

A semi-log plot of the retention times, t_R, of the gases as a function of the reciprocal temperature is presented in Fig. 6. The times plotted have been corrected for temperature and pressure effects, as well as for the dead space in the column. The latter quantity is obtained by passing through the column some gas, e.g., neon (Ne), which is not adsorbed on the column. Thus (Ref. 4),

$$t_R = \frac{3}{2}(t_{obs} - t_{Ne}) \frac{T(P_i/P_o)^2 - 1}{T_0(P_i/P_o)^3 - 1} \qquad (3)$$

where t_{obs} is the observed time; t_{Ne}, is the time it took Ne to traverse the column; T is the column temperature; T_0 is room temperature; and P_i and P_o are the inlet and outlet pressures, respectively.

The resulting straight lines in Fig. 6 are indicative of linear adsorption isotherms and allow comparisons to be made between the two conditions. Nitrogen is seen to behave quite differently on the two columns. On the highly active column (heated to 900°C), the retention of N_2 approaches that of CH_4 at low temperatures; on the less active column, the difference in the retention times of N_2 and CH_4 is approximately constant, and the retention time of N_2 approaches that of O_2 and Ar at the high temperatures.

The observed behavior supports the basic assumptions of the electrostatic theory of physical adsorption. The data also suggest the existence of at least two distinct adsorption sites on the Al_2O_3 surface. On the material heated to 350°C, water blocked the most active surface sites, and the quadrupole–field interaction was not strong enough to perceptively hinder the rotation of N_2. However, when the material is heated to 900°C, water is driven from the most active sites, and the fields over these sites are strong enough to orientate N_2 with its axis perpendicular to the surface. The existence of these sites on the Al_2O_3 surface had been previously suggested (Ref. 2).

4. Conclusion

The results of the chromatographic separations of Ar, O_2, N_2, and CH_4 have been used to support, at least qualitatively, some of the assumptions of the electrostatic theory of physical adsorption. A quantitative treatment of the data is under way to obtain information about barriers to rotation, molecular orientation on the surface, and the distances of the adsorbed molecules from the Al_2O_3 surface.

C. An Explanation of the Gibbs' Phenomenon,

M. M. Saffren

The Gibbs' phenomenon is discussed in nearly every text on mathematical physics and on Fourier series. The phenomenon occurs when one attempts to represent a function that has a jump discontinuity by a Fourier series; the series representation "overshoots" the actual function in the neighborhood of the discontinuity. In this article the Gibbs' phenomenon is shown to be a consequence of two well-known facts: (1) The ordinary eigenfunctions of a linear differential operator form a complete set, and (2) the "torn" or discontinuous eigenfunctions have lower eigenvalues than do the ordinary eigenfunctions. The latter fact is supported by the common observation that a wine glass "rings" at a lower frequency when it is cracked.

Consider now the eigenvalue problem defined by the functional of $\psi(r)$

$$E(\psi) = \frac{\int d\tau \left[|\nabla\psi|^2 + V(\mathbf{r})|\psi|^2 \right]}{\int d\tau |\psi|^2} \tag{1}$$

with the region of integration within some finite closed surface. On this surface, $\psi(r)$ is required to satisfy specified boundary conditions. The eigenfunctions are defined as the functions ψ_n that are the extrema of Eq. (1). The ordinary eigenfunctions are the extrema sought among the class of continuous functions. The "torn" eigenfunctions are the extrema with respect to a different class of functions. A function of this class is discontinuous on some surface which divides the original region in two, but is continuous elsewhere. As is well-known, the torn eigenfunctions have derivatives which vanish at the jump surface when taken normal to the surface. As has already been mentioned, the nth torn eigenfunction has an eigenvalue lower than that of the nth ordinary eigenfunction.

The set of ordinary eigenfunctions, ψ_n, is complete; i.e., if ϕ is a function that obeys the same restrictions as ψ (namely, that it is a continuous function obeying the same boundary conditions as ψ), then

$$S(\phi) = \int d\tau |\phi|^2 = \sum_{n=0}^{\infty} |C_n|^2 \tag{2}$$

$$\mathcal{E}(\phi) = E(\phi) S(\phi) = \sum_{n=0}^{\infty} \lambda_n |C_n|^2 \tag{3}$$

Here, C_n denotes $\int d\tau \phi \psi_n^*$, and λ_n is the eigenvalue of ψ_n (Ref. 5). Though the proof is not included here, it is not difficult to show that, even if ϕ is continuous except at a surface where it jumps, Eq. (2) is true. (The proof is similar to that on p. 157 of Ref. 5.) Thus, if

$$\tilde{\phi} \equiv \sum C_n \psi_n$$

then

$$S(\phi - \tilde{\phi}) = 0 \tag{4}$$

Therefore, the two functions ϕ and $\tilde{\phi}$ are the same in the mean-square. Now, suppose that ϕ is a torn eigenfunction ϕ_0 with the eigenvalue μ_0, and μ_0 is the lowest eigenvalue. As we will show later,

$$E(\phi_0 - \tilde{\phi}_0) \neq 0 \tag{5}$$

If we assume $V(\mathbf{r})$ has an upper bound, then, using Eq. (4), we can show

$$\int d\tau V(\mathbf{r}) |\phi_0 - \tilde{\phi}_0|^2 = 0$$

Thus, we conclude from Eq. (5) that

$$\int d\tau |\nabla(\phi_0 - \tilde{\phi}_0)|^2 \neq 0 \tag{6}$$

If we define

$$[\tilde{\phi}_0]_n \equiv \sum_{k=0}^{n} C_k \psi_k \tag{7}$$

then Eq. (5) shows

$$\lim_{n \to \infty} S(\phi_0 - [\tilde{\phi}_0]_n) \to 0 \tag{8}$$

and Eq. (6) shows

$$\lim_{n \to \infty} \int d\tau |\nabla(\phi_0 - [\tilde{\phi}_0]_n)|^2 \neq 0 \tag{9}$$

Thus, while the sequence $[\tilde{\phi}_0]_n, n = 0, 1, \cdots, \infty$, converges to ϕ_0 in the mean-square, it cannot converge to ϕ_0 point-by-point because of Eq. (6). To see this, let us suppose that $[\tilde{\phi}_0]_n$ converges to a continuous function $[\tilde{\phi}_0]_\infty = \phi_0$. But, if this is true, then

$$\nabla([\tilde{\phi}_0]_\infty - \phi_0) = 0 \tag{10}$$

and Eq. (6) cannot be true. Thus, $[\tilde{\phi}_0]_n$ cannot converge to ϕ_0 everywhere, and, if it does converge everywhere, it cannot converge to a continuous function everywhere.

Eq. (5), used in this argument, will now be shown to be true. We evaluate

$$\mathcal{E}(\phi_0 - [\tilde{\phi}_0]_n) \tag{11}$$

as a sum of two integrals, each integral being taken on each side of the jump surface of ϕ_0. The integration is performed by parts, and the resulting surface integrals

vanish since the normal derivatives of ϕ_0 vanish on the jump surface. We find

$$\mathcal{E}(\phi_0 - [\tilde{\phi}_0]_n) = \mu_0 S(\phi_0) - \mu_0 S(\phi_0, [\tilde{\phi}_0]_n) - \mu_0 S([\tilde{\phi}_0]_n, \phi_0) + \mathcal{E}([\tilde{\phi}_0]_n) \quad (12)$$

$$S(\psi, \phi) \equiv \int d\tau\, \psi^* \phi$$

which can be written as

$$\mu_0 S(\phi_0 - [\tilde{\phi}_0]_n) + \mathcal{E}([\tilde{\phi}_0]_n) - \mu_0 S([\phi_0]_n) \quad (13)$$

If we note that

$$\mathcal{E}([\tilde{\phi}_0]_n) > \lambda_0 S([\tilde{\phi}_0]_n) \quad (14)$$

we see that

$$\lim \mathcal{E}(\phi_0 - [\tilde{\phi}_0]_n) > (\lambda_0 - \mu_0) \lim S([\tilde{\phi}_0]_n) > 0 \quad (15)$$

The next step is to show that any torn eigenfunction ϕ_m yields a Gibbs' phenomenon. To show this, we consider the function

$$\bar{\phi}_m = \phi_m - \sum_{\lambda_n \leq \mu_m} \langle \phi_m | \psi_n \rangle \psi_n \quad (16)$$

This function is ϕ_m orthogonalized to all ψ_n with eigenvalues less than μ_m. If we now evaluate

$$\mathcal{E}([\tilde{\phi}_m]_k - \bar{\phi}_m) \quad (17)$$

we find that

$$\mathcal{E}([\phi_m]_k - \bar{\phi}_m) = \mathcal{E}([\tilde{\phi}_m]_k - \phi_m) = \mathcal{E}([\tilde{\phi}_m]_k) - \mu_m S([\tilde{\phi}_m]_k, \phi_m) \quad (18)$$

However, it is clear that

$$\mathcal{E}([\tilde{\phi}_m]_k) > \lambda_m S([\tilde{\phi}_m]_k) \quad (19)$$

But, since $\lambda_m > \mu_m$, we finally see that

$$\mathcal{E}([\tilde{\phi}_m]_k - \phi_m) > 0 \quad (20)$$

As demonstrated above, this is all we need to show that a function, here ϕ_m, exhibits a Gibbs' phenomenon.

We can now demonstrate that any torn function ψ manifests a Gibbs' phenomenon. All we need show is that

$$\mathcal{E}(\tilde{\psi}) > \mathcal{E}(\psi) \quad (21)$$

The remaining steps are the same as those in the demonstration that ϕ_n manifests a Gibbs' phenomenon To prove Eq. (21), we expand ψ in the torn eigenfunctions appropriate to the tear in ψ. We denote the expansion up to the nth torn eigenfunction as $[\hat{\psi}]_n$. It is well-known that $\mathcal{E}(\hat{\psi}) = \mathcal{E}(\psi)$. Since we have shown above that, for any torn eigenfunction,

$$\mathcal{E}(\tilde{\phi}_n) > \mathcal{E}(\phi_n) \quad (22)$$

clearly then this is also true for any linear combination of the torn eigenfunctions. Thus,

$$\mathcal{E}([[\tilde{\hat{\psi}}]_n]_k) > \mathcal{E}([\hat{\psi}]_n) \quad (23)$$

and so

$$\mathcal{E}([\tilde{\hat{\psi}}]_k) > \mathcal{E}(\hat{\psi}) \quad (24)$$

But, it is easy to show that

$$\mathcal{E}(\tilde{\psi}) \geq \mathcal{E}([\tilde{\hat{\psi}}]_k) \quad (25)$$

Therefore, since $\mathcal{E}(\psi) = \mathcal{E}(\hat{\psi})$, we have what we set out to prove:

$$\mathcal{E}(\tilde{\psi}) > \mathcal{E}(\psi) \quad (26)$$

In this article, we have shown that the Gibbs' phenomenon is a result of trying to expand a mode of low frequency (or energy) in a linear combination of modes, each having a higher frequency (or energy) than the mode we are attempting to represent. This is most clear when the mode is the lowest torn eigenfunction, which has a frequency lower than any ordinary mode. The Gibbs' phenomenon is a manifestation of how the expansion accommodates two conflicting requirements: (1) that the expansion for the torn mode converge in the mean-square to the torn mode itself, and (2) that the expansion have a higher mean frequency than the mode it represents. The accommodation is achieved by the expansion developing a discontinuity which leads to a discontinuous gradient. It is this discontinuity in gradient that keeps the mean frequency of the expansion higher than the frequency of the mode it represents, while simultaneously allowing the expansion to converge to this mode in the mean-square.

D. Relativistic Collapse to a Schwarzschild Sphere,[1]

H. D. Wahlquist and F. B. Estabrook

1. Introduction

The interior Schwarzschild solution describing a static (rigid, non-rotating) sphere of perfect fluid at constant density is the simplest analytic metric known for a finite gravitating body. It has not usually been noted that the field equations allow an arbitrary function of time to be introduced into this metric without destroying the properties of simplicity, rigidity, and constant density, but resulting in a time-dependent pressure field (see, however, Ref. 6). We have exploited this time-dependence to construct idealized models of spherically symmetric, non-static processes, such as accretion or relativistic collapse onto a central body. The models are of sufficient simplicity to permit an exact analytical solution of the entire gravitational problem, making comparison of the predictions of general relativity with Newtonian and post-Newtonian theory for the dynamics of the models unambiguous, even in extreme relativistic regimes.

The complete solutions are obtained by piecing together three different, well-known, space–time metrics across surfaces of discontinuity. All junction conditions required by the Lichnerowicz postulate of admissible coordinates (Ref. 7) are satisfied. The metrics, however, are expressed in "non-admissible" comoving coordinates, and the fitting is actually accomplished using these coordinates and the tetrad or dyadic formulation of the junction conditions.[2]

The three metrics employed are: (I) the interior Schwarzschild with constant density ρ_s but time-dependent pressure, (II) the Oppenheimer–Snyder solutions (Ref. 8) for the spherically symmetric motion of incoherent matter, and (III) the exterior Schwarzschild. Fig. 7 is a schematic space–time diagram of the simplest combination of these. It represents a contracting spherical dust cloud (region II, outer boundary Σ_1) which is condensing and accreting on the surface Σ_3 of a growing Schwarzschild sphere (region I, below dashed line) to build the final configuration, a static Schwarzschild sphere of radius r_m (region I, above dashed line, boundary Σ_2). On Σ_3, the matter undergoes a phase transformation from the incoherent state of zero pressure and varying density

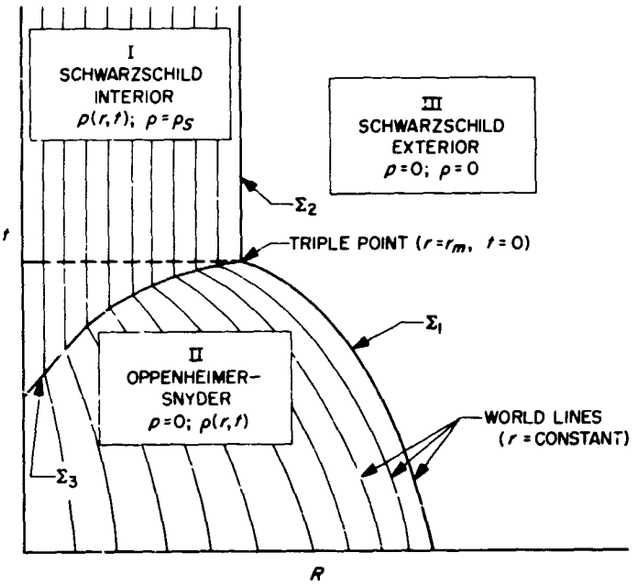

Fig. 7. Contraction of dust cloud to Schwarzschild sphere

to the interior state of variable pressure and constant density ρ_s. Some other possible mosaics of these metrics are shown in Fig. 8; their analytical descriptions can also be constructed using the dyadic methods.

The general dyadic equations for timelike congruences (Refs. 9 and 10) are specialized for the present case by imposing several conditions. The matter is to be non-rotating ($\Omega = 0$), and we shall adopt non-rotating axes ($\omega = 0$). Spherical symmetry is imposed by representing the only distinguished spatial direction at every point with a unit, radial, 3-vector $\hat{\mathbf{u}}$ and expressing all vectors and dyadics in terms of it. The remaining kinematical variables of the matter then take the forms

$$\left.\begin{aligned} \mathbf{a} &= a\hat{\mathbf{u}} \\ \mathbf{S} &= \frac{1}{3}\theta\mathbf{I} + \sigma(\mathbf{I} - 3\hat{\mathbf{u}}\hat{\mathbf{u}}) \end{aligned}\right\} \tag{1}$$

where a is the absolute acceleration, θ is the expansion, and σ is the shear. Similarly, the electric and magnetic components of the Weyl tensor, represented by two symmetric traceless dyadics, must have the forms

$$\left.\begin{aligned} \mathbf{A} &= \alpha(\mathbf{I} - 3\hat{\mathbf{u}}\hat{\mathbf{u}}) \\ \mathbf{B} &= \beta(\mathbf{I} - 3\hat{\mathbf{u}}\hat{\mathbf{u}}) \end{aligned}\right\} \tag{2}$$

[1]A paper on this subject, including a more detailed derivation of results than that presented here, has been accepted for publication in *The Physical Review*.

[2]Estabrook, F. B., and Wahlquist, H. D., *Tetrad Formulation of Junction Conditions in General Relativity* (in press); cf, SPS 37-41, Vol. IV, p. 189.

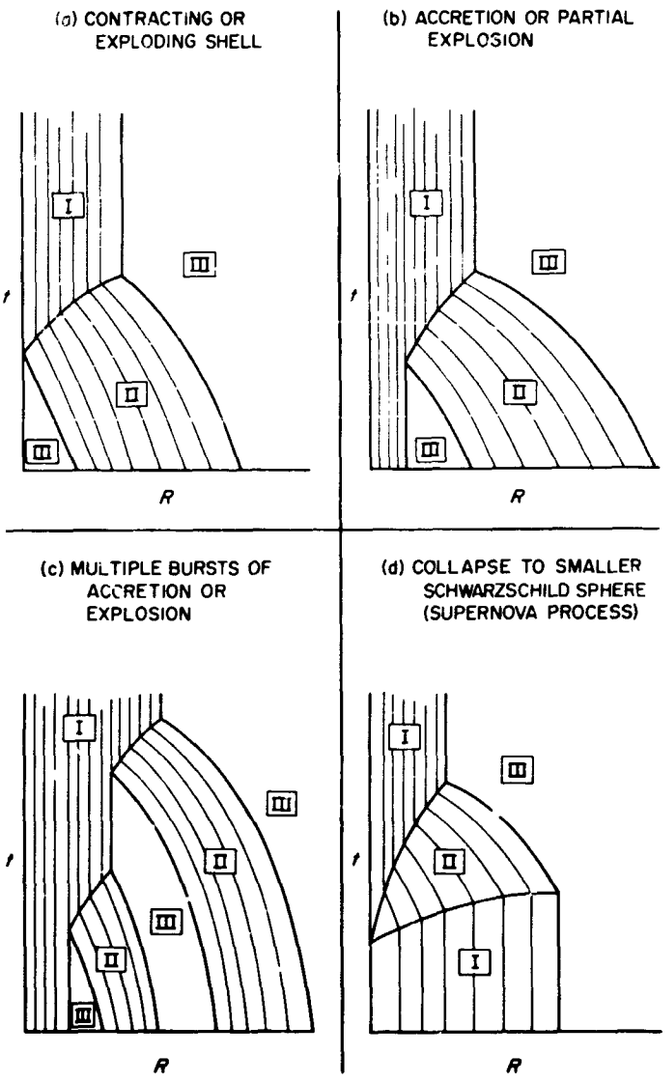

Fig. 8. Other processes employing the same metrics as Fig. 7

It can be shown from the equations that, in fact, in the present case $\beta = 0$. Finally, for a comoving frame of reference, the momentum density vanishes ($t = 0$), while the remaining components of the Einstein tensor will include the local proper energy density ρ and the stress dyadic for a perfect fluid

$$\mathsf{T} = -p\mathsf{I} \tag{3}$$

Each of the three regions used in these models is characterized by different further specializations. In region I, we want to describe a rigid fluid with constant density ($\theta = \sigma = \dot{\rho} = \rho' = 0$), and, since the space–time of the interior Schwarzschild solution is conformally flat, we also have $\alpha = 0$. For the incoherent matter of region II, we put $p = a = 0$. In region III, which being empty offers no physically preferred timelike congruence, we adopt the timelike isometry for our reference frame so that, in addition to $p = \rho = 0$, we have $\theta = \sigma = 0$, and all time derivatives vanish.

If we now introduce comoving spatial coordinates (r, ψ, χ), the spherical metric can be written in the form

$$ds^2 = -\frac{1}{\phi^2}\,dt^2 + \frac{1}{\delta^2}\,dr^2 + R^2\,(d\psi^2 + \sin^2\psi\, d\chi^2) \tag{4}$$

where R denotes the usual radial curvature coordinate and ϕ, δ, and R are functions of r and t only. Inserting the appropriate assumptions, the dyadic differential equations can be solved for the metric coefficients ϕ, δ, and R for each of the three regions. In region I, the solution is unique up to an arbitrary function of time only, $F(t)$; in region II, three arbitrary functions of r only, $f(r)$, $g(r)$, and $h(r)$, remain; in region III, the solution is unique.

Having obtained the metrics and physical quantities for each region expressed in terms of intrinsic comoving coordinates, the remaining task is to join them together properly at the three surfaces of discontinuity Σ_1, Σ_2, and Σ_3. The problem is usually formulated theoretically in terms of admissible coordinates (Ref. 7), for which the metric tensor itself and its first derivatives are *everywhere* continuous. When such coordinates can be discovered, the matching problem is quite simple. In general, of course, the comoving coordinates used here will not satisfy the requirements of admissibility. To proceed, however, by searching for a set of admissible coordinates valid for all three regions leads to considerable difficulties. Not the least of these difficulties arise from the facts that the metrics of regions I and II are not explicit, but involve several functions as yet arbitrary, and that the forms of the boundary surfaces themselves are not yet completely specified. In practice, this problem can be handled in a quite straightforward manner by turning to a tetrad or dyadic formulation of the junction conditions which can be specially adapted to the matching of metrics expressed in comoving coordinates. The general formalism of this approach has been developed (see Footnote 2), and it has been shown that the continuity conditions used below are equivalent to, and in fact guarantee, the existence of admissible coordinates without explicitly employing them.

When the 29 general dyadic junction conditions of the general formalism for motion normal to spatial boundaries are written for spherical symmetry and comoving

frames of reference, the following set of 7 continuity conditions results:

$$\frac{\cot\psi}{R} \tag{5a}$$

$$\gamma\left[\eta + v\left(\frac{1}{3}\theta + \sigma\right)\right] \tag{5b}$$

$$\gamma\left[v\eta + \frac{1}{3}\theta + \sigma\right] \tag{5c}$$

$$\gamma\left[\gamma^2 vv' + \gamma^2\dot{v} + a + v\left(\frac{1}{3}\theta - 2\sigma\right)\right] \tag{5d}$$

$$\gamma^2 v\,(p + \rho) \tag{5e}$$

$$\gamma^2\,[v^2\rho + p] \tag{5f}$$

$$\frac{1}{3}\rho + \alpha \tag{5g}$$

Each of these expressions must be continuous across the boundary. The quantity v is the proper, radial 3-velocity of the moving spherical 2-surface, as observed from the comoving frame of reference on each side, and $\gamma = (1 - v^2)^{-1/2}$. We assume throughout that the angular coordinates ψ and χ are propagated continuously across all boundaries, so the first expression simply requires that R also be everywhere continuous. Conditions (5a)–(5d) ensure that the intrinsic first and second fundamental forms of the boundary are unique. Conditions (5e) and (5f) are the usual relativistic Rankine–Hugoniot relationships in a symmetric form, and Condition (5g) requires continuity of a certain combination of curvature components involving both Einstein and Weyl tensors.

These conditions are now applied to each of the three surfaces of discontinuity to determine the arbitrary functions $F(t)$, $f(r)$, $g(r)$, and $h(r)$. However, when completed, we find that we are still left with two functions of r on the boundary Σ_3 which remain arbitrary. In other words, for each choice of two such functions and the two parameters ρ_s and r_m, we obtain a unique solution for a model of the type depicted in Fig. 7. The physical significance of this is perhaps most clearly seen by interpreting the functions as: (1) the amount of matter crossing Σ_3 and accreting in region I per unit time, and (2) the velocity of impact of this matter at Σ_3. Since we impose no thermodynamic constraints at Σ_3 other than the local conservation of energy–momentum given by the Rankine–Hugoniot relationships, both of these quantities can be specified. Recalling the definition of the velocities appearing in the junction conditions, the two quantities can be written as $\rho_s v_I$ and

$$(v_I - v_{II})/(1 - v_I v_{II}),$$

respectively: so, it is convenient to adopt as arbitrary functions the two velocities

$$u(r) \equiv v_I \tag{6}$$

the velocity of the surface of the growing sphere, and

$$v(r) \equiv \frac{v_I - v_{II}}{1 - v_I v_{II}} \tag{7}$$

the velocity of impact of the dust, both relative to the static matter of region I.

2. Metrics of Fig. 7

We shall now present a summary of the metrics and physical quantities for the type of models depicted in Fig. 7. The solutions are specified by the two velocity functions $u(r)$ and $v(r)$ on Σ_3, which are arbitrary to within some broad constraints discussed later, and it is convenient to define

$$u_m = u(r_m), \qquad v_m = v(r_m) \tag{8}$$

The equations as written are equally valid for either contracting or expanding models.

The space–time metrics and physical quantities in the three regions of Fig. 7 are as follows:

Region I.

$$ds^2 = -\frac{1}{4}\left[3F(t_I) - \left(1 - \frac{2}{3}\rho_s r^2\right)^{1/2}\right]^2 dt_I^2 + \left[1 - \frac{2}{3}\rho_s r^2\right]^{-1} dr^2 + r^2 d\Omega^2 \tag{9}$$

with

$$F(t_I) = \left(1 - \frac{2}{3}\rho_s r^2\right)^{1/2}\left[\frac{1 - u(r)\,v(r)}{1 - 3u(r)\,v(r)}\right]\Bigg|_{r = r_{\Sigma_3}(t_I)}, \qquad t_I < 0$$
$$= \left(1 - \frac{2}{3}\rho_s r_m^2\right)^{1/2}, \qquad t_I > 0 \tag{10}$$

The inequalities here would reverse for an expanding motion. The function of r in the first expression for F is converted to a function of t_I by means of the equation of the boundary Σ_3:

$$t_I = -\int_r^{r_m} \frac{[1 - 3u(x)\,v(x)]}{u(x)\left[1 - \frac{2}{3}\rho_s x^2\right]}\,dx \tag{11}$$

Letting $d\Sigma_3$ represent an interval on the surface Σ_3, we find

$$d\Sigma_3^2 = -\frac{(1 - u^2)}{u^2\left(1 - \frac{2}{3}\rho_s r^2\right)}\,dr^2 + r^2 d\Omega^2 \tag{12}$$

The equation for the boundary Σ_2 is simply $r = r_m$. Its intrinsic metric is

$$d\Sigma_2^2 = -\left(1 - \frac{2}{3}\rho_s r_m^2\right)dt_I^2 + r_m^2 d\Omega^2 \tag{13}$$

The pressure field in region I is given by

$$p(r, t_I) = \rho_s\left\{\frac{\left(1 - \frac{2}{3}\rho_s r^2\right)^{1/2} - F(t_I)}{3F(t_I) - \left(1 - \frac{2}{3}\rho_s r^2\right)^{1/2}}\right\} \tag{14}$$

and, on the boundaries,

$$p_{\Sigma_3} = -\rho_s u v\,, \qquad p_{\Sigma_2} = 0 \tag{15}$$

Region II.

$$ds^2 = -dt_{II}^2 + \frac{(1 - v^2)}{\left(1 - \frac{2}{3}\rho_s r^2\right)}\left(\frac{\partial R}{\partial r}\right)^2 dr^2 + R^2 d\Omega^2 \tag{16}$$

with $R(r, t_{II})$ given implicitly by

$$t_{II} = \frac{v}{|v|}\int_r^R \left[\frac{v^2(r) - \frac{2}{3}\rho_s r^2}{1 - v^2(r)} + \frac{2}{3}\rho_s \frac{r^3}{x}\right]^{-1/2} dx - \int_r^{r_m} \frac{[1 - u(x)\,v(x)]\,dx}{u(x)\,[1 - v^2(x)]^{1/2}\left(1 - \frac{2}{3}\rho_s x^2\right)^{1/2}} \tag{17}$$

and

$$\frac{\partial R}{\partial r} = \left(\frac{v^2 - \frac{2}{3}\rho_s r^2}{1 - v^2} + \frac{2}{3}\rho_s \frac{r^3}{R}\right)^{1/2} \left\{ \frac{(u - v)}{|v|\, u (1 - v^2)^{1/2} \left(1 - \frac{2}{3}\rho_s r^2\right)^{1/2}} \right.$$

$$\left. + \int_r^R \left(\frac{v^2 - \frac{2}{3}\rho_s r^2}{1 - v^2} + \frac{2}{3}\rho_s \frac{r^3}{x}\right)^{-3/2} \left[\rho_s \frac{r^2}{x} + \frac{1}{2}\frac{d}{dr}\left(\frac{v^2 - \frac{2}{3}\rho_s r^2}{1 - v^2}\right)\right] dx \right\} \tag{18}$$

The equations for the boundaries of region II are: for Σ_3, $r = R$, or, from Eq. (17),

$$t_{II} = -\int_r^{r_m} \frac{[1 - u(x)\, v(x)]}{u(x)\, [1 - v^2(x)]^{1/2} \left(1 - \frac{2}{3}\rho_s x^2\right)^{1/2}} dx \tag{19}$$

giving Eq. (12) again for $d\Sigma_3^2$; and for Σ_1, $r = r_m$, so that

$$d\Sigma_1^2 = -dt_{II}^2 + R^2(r_m, t_{II})\, d\Omega^2 \tag{20}$$

or, again using Eq. (17),

$$d\Sigma_1^2 = -\left[\frac{v_m^2 - \frac{2}{3}\rho_s r_m^2}{1 - v_m^2} + \frac{2}{3}\rho_s \frac{r_m^3}{R}\right]^{-1} dR^2 + R^2 d\Omega^2 \tag{21}$$

The proper density in region II is given by

$$\rho(r, t_{II}) = \rho_s \frac{r^2}{R^2}\left(\frac{\partial R}{\partial r}\right)^{-1} \tag{22}$$

and, on Σ_3,

$$\rho_{\Sigma_3} = \rho_s \frac{u(1 - v^2)}{(u - v)} \tag{23}$$

Region III.

$$ds^2 = -\left(1 - 2\frac{M}{R}\right) dt_{II}^2 + \left(1 - 2\frac{M}{R}\right)^{-1} dR^2 + R^2 d\Omega^2 \tag{24}$$

with

$$M = \frac{1}{3}\rho_s r_m^3 \tag{25}$$

The boundary equations for this region are: for Σ_2, $R = r_m$, giving Eq. (13) for $d\Sigma_2^2$ (with $t_I = t_{III}$ on Σ_2); and for Σ_1,

$$t_{III} = \frac{v}{|v|} \frac{\left(1 - \frac{2}{3}\rho_s r_m^2\right)^{1/2}}{(1 - v_m^2)^{1/2}} \int_{r_m}^{R} \left[\frac{v_m^2 - \frac{2}{3}\rho_s r_m^2}{1 - v_m^2} + \frac{2}{3}\rho_s \frac{r_m^3}{x}\right]^{-1/2} \left[1 - \frac{2}{3}\rho_s \frac{r_m^3}{x}\right]^{-1} dx \tag{26}$$

giving Eq. (21) again for $d\Sigma_1^2$.

Certain constraints must be imposed on the parameters and velocities if these solutions are to be complete and everywhere regular with no further boundaries. First, to describe the situation of Fig. 7 rather than that of Fig. 8(a), we must choose $v(0) = 0$. Second, to ensure that $0 \leqq p(r, t_I) < \infty$, we must have

$$0 \leqq (-uv) < \frac{\left[3\left(1 - \frac{2}{3}\rho_s r^2\right)^{1/2} - 1\right]}{3\left[1 - \left(1 - \frac{2}{3}\rho_s r^2\right)^{1/2}\right]} \tag{27}$$

From this, it follows that

$$\frac{2}{3}\rho_s r_m^2 < \frac{8}{9} \tag{28}$$

which is the usual limit for the interior Schwarzschild solution. Next, from Eq. (22), we must have $\partial R/\partial r > 0$; thus, from the first factor of Eq. (18),

$$\frac{2}{3}\rho_s r^2 \leqq v^2 < 1 \tag{29}$$

The inequality on the left-hand side above may be rewritten in an obvious notation as an energy constraint

$$\frac{1}{2}v^2 - \frac{M(r)}{r} \geqq 0 \tag{30}$$

required to ensure that the matter of region II comes from (or goes to) infinite distance. The second factor of Eq. (18) must also be prevented from vanishing, which it might do if

$$\frac{d}{dr}\left[\frac{v^2 - \frac{2}{3}\rho_s r^2}{1 - v^2}\right] \tag{31}$$

became sufficiently negative (all other terms of the factor being positive). Such behavior of the energy on Σ_3 leads to shells of matter overtaking others (intersection of the world lines in region II), violating the assumption of incoherent matter in region II.

It may be noted from Eq. (10) that, in general, a discontinuity of the pressure in region I occurs at the surface $t_I = 0$ (the dashed line of Fig. 7). Physically, this would appear as a shock wave of infinite speed, resulting from the sudden cessation of accretion at $r = r_m$. The discontinuity is removed by setting $u_m = 0$, which corresponds simply to vanishing density at the outer boundary of the collapsing cloud, as is evident from Eq. (23). Letting $u(r) = 0$ anywhere, however, gives rise to some difficulties with the coordinate r in region II and on Σ_3 at such points. These can be handled by using instead a new coordinate $\bar{r}$, defined, for instance, by

$$d\bar{r} = (\rho_{\Sigma_3})^{-1} dr$$

For arbitrary choices of the functions $u(r)$ and $v(r)$, satisfying the foregoing constraints and $u_m = 0$, the models may still have the acausal feature that the surfaces of constant pressure in region I are spacelike. This is a result of the incompressibility of the matter in region I and is not surprising. For such fluids, in the words of Sommerfeld (Ref. 11), the pressure takes on the rather unphysical character of a "Lagrangian multiplier... a reaction against the condition of incompressibility... without energetic consequence." Nevertheless, here its contribution to the gravitational field is fully included.

E. Particular Solutions of a System of Nonlinear First-Order Ordinary Differential Equations,

J. S. Zmuidzinas

Let E_p be the Euclidean space of all p-vectors $x = (x^1, \cdots, x^p)$, $-\infty < x^i < \infty$. Consider the system of p ordinary differential equations

$$\dot{x}^i = X^i(x) \tag{1}$$

where

$$\dot{x}^i \equiv dx^i/dt$$

and the x^i are given functions of $x = x(t)$. The parameter t is supposed to lie in the interval $[0, \infty)$. It is assumed that the x^i are not explicit functions of t, i.e., that $\partial X^i/\partial t = 0$.

Particular solutions of Eq. (1) can be obtained from the knowledge of a set of invariant relations (IRs) defined as follows: Let $f_0(x)$ be some function of the x^i which is differentiable a sufficient number of times. Introduce the operator

$$\nabla \equiv X^i \partial_i = d/dt$$

where

$$\partial_i = \partial/\partial x^i$$

and put

$$f_n(x) = \nabla^n f_0(x), \qquad n = 0, 1, 2, \cdots$$

Suppose it happens that each $f_m, m > n$, vanishes identically if we set $f_0(x) = f_1(x) = \cdots = f_n(x) = 0$. Then, we say that the set $\{f_k(x) = 0, k = 0, 1, 2, \cdots, n\}$ is a set of IRs.

It is easy to find a characterization of an f_{n+1} vanishing when $f_k(x) = 0, k = 0, \cdots, n$. It is sufficient to demand that f_{n+1} be linear in the f_k:

$$f_{n+1}(x) = \sum_{k=0}^{n} a_k(x) f_k(x) \tag{2}$$

where the a_k are some functions of x nonsingular at the "point" $(f_0(x), \cdots, f_n(x)) = 0$ (a variety in E_p). If f_{n+1} is given by Eq. (2), then all $f_m, m > n + 1$, are also of this form. To see this, we use

$$\nabla f_k = f_{k+1}, \qquad k = 0, 1, 2, \cdots, n-1$$

$$= \sum_{l=0}^{n} a_l f_l, \qquad k = n$$

in deducing that

$$\begin{aligned} f_{n+2} &= \nabla f_{n+1} \\ &= \nabla\left(\sum_{k=0}^{n} a_k f_k\right) \\ &= \sum_{k=0}^{n} (\nabla a_k \cdot f_k + a_k \cdot \nabla f_k) \\ &= \sum_{k=0}^{n} (\nabla a_k + a_{k-1} + a_n a_k) f_k \end{aligned}$$

where $a_{-1} \equiv 0$. Similar arguments establish our assertion for all f_m with $m > n + 2$.

Starting with an arbitrary f_0, there need not exist a finite integer n for which Eq. (2) is true. On the other hand, there may exist many different functions $f_0^{(1)}, f_0^{(2)}, \cdots$ for which Eq. (2) holds, with various integers $n^{(1)}, n^{(2)}, \cdots$. The $f_0^{(i)}$ with the smallest $n^{(i)}$ are of particular interest.

To illustrate the utility of IRs, consider the system

$$\dot{x} = x^2 + y^2 \tag{3}$$

$$\dot{y} = 2xy \tag{4}$$

Suppose we try

$$f_0(x, y) = x + y \tag{5}$$

Then,

$$\begin{aligned} f_1(x, y) &= \{(x^2 + y^2)\partial_x + 2xy\partial_y\} f_0(x, y) \\ &= (x + y)^2 \\ &= [f_0(x, y)]^2 \end{aligned}$$

Thus, $f_0(x, y) \equiv x + y = 0$ is an IR. Imposing $f_0 = 0$ on our system of differential equations, we obtain

$$\dot{x} = 2x^2$$

$$\dot{y} = -2y^2$$

The solutions are elementary:

$$x = \tfrac{1}{2}(c - t)^{-1}$$

$$y = -\tfrac{1}{2}(c - t)^{-1}$$

Here, c is an arbitrary constant. These solutions are special cases of the more general solution obtained by adding equations for x and y:

$$\dot{f}_0 = f_0^2$$

$$f_0 \equiv x + y = (c - t)^{-1}$$

We may use $f_0 = x + y \neq 0$ to eliminate, say, y from Eq. (3), thus obtaining

$$\dot{x} = 2x^2 - 2xf_0 + f_0^2 \tag{6}$$

Putting

$$x = f_0 u$$

substituting into Eq. (6), and using $\dot{f}_0 = f_0^2$, we obtain

$$\dot{u} = f_0 (2u^2 - 3u + 1) \tag{7}$$

The solution of this equation follows by quadrature:

$$u = \frac{c' - f_0/2}{c' - f_0}$$

Thus, we have found, with the help of $f_1 = \dot{f}_0 = f_0^2$, the family of solutions

$$x = f_0 u$$

$$y = f_0 - x = f_0 (1 - u)$$

Let us now consider a more general system of equations, still homogeneous:

$$\dot{x} = ax^2 + bxy + cy^2 \equiv X$$

$$\dot{y} = dx^2 + exy + fy^2 \equiv Y \tag{8}$$

The homogeneity of X and Y suggests looking for homogeneous IRs. The simplest choice for f_0 is the linear expression

$$f_0 = x + \alpha y \tag{9}$$

We compute $f_1 = \nabla f_0$ and eliminate x from f_1 by means of Eq. (9). The result is

$$f_1 = [d\alpha^3 + (a - e)\alpha^2 + (f - b)\alpha + c] y^2 - [2d\alpha^2 + (2a - e)\alpha - b] y f_0 + (d\alpha + a) f_0^2 \tag{10}$$

In order that $f_1 = 0$ when $f_0 = 0$, we must require that the coefficient of y^2 vanish. This requirement yields the following cubic equation for the parameter α:

$$d\alpha^3 + (a - e)\alpha^2 + (f - b)\alpha + c = 0 \tag{11}$$

The three solutions $\alpha_{1,2,3}$ of this equation yield the desired f_0's:

$$f_0^{(i)}(x, y) = x + \alpha_i y, \qquad i = 1, 2, 3$$

For the special case $a = c = 1$, $b = d = f = 0$, and $e = 2$, we find $\alpha = \pm 1$ and so

$$f_0^{(1)} = x + y$$

$$f_0^{(2)} = x - y$$

Here, $f^{(1)}$ is just Eq. (5), while $f^{(2)}$ leads to new particular solutions.

While it is true that $f_0 = 0$ entails $f_1 = 0$, it is not necessarily true that $f_0 = f_0(t)$ yields f_1 independent of y, unless the coefficient of yf_0 in Eq. (10) happens to vanish. The necessary conditions for this coefficient to vanish are found to be

$$e\alpha^2 + (b - 2f)\alpha - 2c = 0, \qquad \alpha \neq 0$$

or

$$b = 0, \qquad \alpha = 0$$

In general, neither of these conditions will be satisfied.

Let us now choose a homogeneous quadratic expression for f_0:

$$f_0 = (x + \alpha y)(x + \beta y) \tag{12}$$

Then,

$$f_1 = (X + \alpha Y)(x + \beta y) + (x + \alpha y)(X + \beta Y)$$

If $f_0 = 0$, then either $x + \alpha y = 0$ or $x + \beta y = 0$. Suppose the former is the case. Then,

$$f_1 = [X + \alpha Y]_{x=-\alpha y}(\beta - \alpha)\, y$$

vanishes if $\beta = \alpha$ (the trivial case) or if

$$[X + \alpha Y]_{x=-\alpha y} = 0$$

But, in the latter case, α must satisfy Eq. (11), and so we are back at the linear case already discussed. Since Eq. (12) is symmetric in α and β, the same conclusion obtains if $x + \beta y = 0$. We see then that choosing Eq. (12) does not lead to new solutions. Obviously, the same is true of higher-degree homogeneous polynomial expressions for f_0.

Our results for Eq. (8) may be generalized in several ways. First, suppose we have the system

$$\dot{x} = a_0 x^n - a_1 x^{n-1} y + a_2 x^{n-2} y^2 + \cdots + (-)^n a_n y^n$$

$$\dot{y} = b_0 x^n - b_1 x^{n-1} y + b_2 x^{n-2} y^2 + \cdots + (-)^n b_n y^n$$

Then, it is easy to show that

$$f_0 = x + \alpha y = 0$$

is an IR, provided α satisfies

$$b_0 \alpha^{n+1} + (a_0 + b_1)\alpha^n + (a_1 + b_2)\alpha^{n-1}$$

$$+ \cdots + (a_{n-1} + b_n)\alpha + a_n = 0$$

Next, we generalize our results to an arbitrary number of variables $x^i, i = 1, 2, \cdots, p$. We take as our system

$$\dot{x}^i = a^i_{j_1 \cdots j_n} x^{j_1} \cdots x^{j_n} \equiv X^i$$

$$(i, j_1, \cdots, j_n = 1, 2, \cdots, p) \qquad (13)$$

The homogeneity of the X^i suggests the ansatz

$$x^i = \alpha^i z^\nu, \qquad (14)$$

where α^i and ν are nonzero constants. Substituting this into Eq. (13), we find

$$\dot{z} = a^i_{j_1 \cdots j_n} \frac{\alpha^{j_1} \cdots \alpha^{j_n}}{\nu \alpha^i} z^{(n-1)\nu + 1} \quad \text{(no sum on } i\text{)}$$

For consistency, we demand that the coefficient of $z^{(n-1)\nu+1}$ be independent of i:

$$-\lambda \equiv a^1_{j_1 \cdots j_n} \frac{\alpha^{j_1} \cdots \alpha^{j_n}}{\nu \alpha^1} = \cdots = a^p_{j_1 \cdots j_n} \frac{\alpha^{j_1 \cdots j_n}}{\nu \alpha^p} \qquad (15)$$

Then,

$$\dot{z} = -\lambda z^{(n-1)\nu + 1}$$

Hence,

$$\left.\begin{aligned} z(t) &= [(n-1)\nu(c + \lambda t)]^{-(n-1)^{-1}\nu^{-1}}, && n \neq 1 \\ &= c' e^{-\lambda t}, && n = 1 \end{aligned}\right\} \qquad (16)$$

The $n - 1$ equations for the $n - 1$ ratios $\bar{\alpha}^j = \alpha^j/\alpha^1$, say, are coupled algebraic of order $n + 1$ in the $\bar{\alpha}$'s.

Define the function

$$g(x) = \beta_i x^i \qquad (17)$$

where the β_i are so far arbitrary. With Eq. (14), this becomes

$$g = \rho z^\nu$$

$$\rho \equiv \alpha^i \beta_i$$

We also have

$$X^i = \dot{x}^i = \nu \alpha^i z^{\nu-1} \dot{z} = -\nu \lambda \alpha^i z^{n\nu}$$

Therefore,

$$\begin{aligned}\nabla g &= \beta_i X^i \\ &= -\nu\lambda\rho z^{n\nu} \\ &= -\nu\lambda z^{(n-1)\nu} g\end{aligned}$$

Clearly, $g = 0$ implies $\nabla g = 0$. Thus, we may identify g with f_0:

$$f_0(x) = \beta_i x^i = \rho z^\nu$$

Taking $f_0 = 0$ means $\rho = 0$, since the other possibility $z \equiv 0$ is trivial. The $f_0 = 0$ solutions are thus those with $x^i = \alpha^i z^\nu$, where z is given by Eq. (16). The β_i are no longer arbitrary, but constrained by $\rho = \alpha^i \beta_i = 0$. A more general class of solutions is obtained by taking $\rho \neq 0$. Then, $f_0 = \rho z^\nu$ or

$$\beta_i x^i(t) = \rho [z(t)]^\nu$$

Suppose $\beta_p \neq 0$ (relabel if necessary). Then, we may solve for x^p and eliminate it from our original system of Eq. (13) in favor of $x^1, \cdots, x^{p-1}$ and the known function z, thus reducing the number of unknown functions to $p - 1$. Making the further substitution $x^i = z^\nu y^i$, $i = 1, 2, \cdots, p-1$, we can cast these equations in a form similar to Eq. (7), which may, in certain cases, be amenable to solution or further reduction.

Work on further generalizations to nonhomogeneous X^i is in progress and will be reported later.

References

1. Baker, E. B., Burd, L. W., and Root, G. N., *Review of the Scientific Institute,* Vol. 34, p. 243, 1963.
2. King, J., Jr., and Benson, S. W., *Journal of Chemical Physics,* Vol. 44, 1007, 1966.
3. Hirschfelder, Curtis, and Bird, *Molecular Theory of Gases and Liquids,* John Wiley and Sons, Inc., New York, 1954.
4. Littlewood, A. B., *Gas Chromatography,* Chap. 2, Academic Press, New York, 1962.
5. Courant, R., and Hilbert, D., *Methods of Mathematical Physics,* Vol. I, p. 157, Interscience Publishers, New York, 1957.
6. Taub, A. H., *Recent Developments in General Relativity,* p. 449, Macmillan Co., New York, 1962.
7. Lichnerowicz, A., *Theories Relativistes de la Gravitation et de l'Electromagnetisme,* Masson et Cie., Paris, 1955.
8. Oppenheimer, J. R., and Snyder, H., *Physical Review,* Vol. 56, p. 455, 1939.
9. Estabrook, F. B., and Wahlquist, H. D., "Dyadic Analysis of Space–Time Congruences," *Journal of Mathematical Physics,* Vol. 5, p. 1629, 1964.
10. Wahlquist, H. D., and Estabrook, F. B., "Rigid Motions in Einstein Spaces," *Journal of Mathematical Physics,* Vol. 7, p. 894, 1966; also published as Technical Report 32-868, Jet Propulsion Laboratory, Pasadena, California, 1966.
11. Sommerfeld, A., *Mechanics of Deformable Bodies,* p. 91, Academic Press, Inc., New York, 1950.